Short communication

Nanocomposite C/Li$_2$MnSiO$_4$ cathode material for lithium ion batteries

M. Świętosławski, M. Molenda*, K. Furczoń, R. Dziembaj

Jagiellonian University, Faculty of Chemistry, Ingardena 3, 30-060 Krakow, Poland

HIGHLIGHTS

- C/Li$_2$MnSiO$_4$ nanocomposite was obtained by sol−gel method and carbon coating process.
- Fine and uniform carbon nanocoatings on nanometric Li$_2$MnSiO$_4$ material were obtained.
- Amorphous Li$_2$MnSiO$_4$ was formed during electrochemical process.
- D$_{Li+}$ was calculated for charged and discharged C/Li$_2$MnSiO$_4$ material.
- C/Li$_2$MnSiO$_4$ nanocomposite revealed high discharge capacity 185 mA h g^{-1} at 1.5−4.8 V.

ARTICLE INFO

ABSTRACT

C/Li$_2$MnSiO$_4$ nanocomposite material was obtained by sol−gel method followed by carbon coating process. Electrochemical properties of nanosized C/Li$_2$MnSiO$_4$ cathode composite were studied in terms of changes in the long range ordering of the crystalline structure. Structural morphology was determined using X-ray diffraction (XRD) and transmission electron microscopy (TEM). Ex-situ XRD studies confirmed amorphization of material during electrochemical process. Even though, C/Li$_2$MnSiO$_4$ composite revealed high discharge capacity (up to 185 mAh g^{-1}) within 1.5−4.8 V, what corresponds to the exchange of more than one lithium-ion per formula unit (1.11 mole Li$^+$). Electrochemical impedance spectroscopy (EIS) studies showed substantial changes in electrical properties of Li$_2$MnSiO$_4$ during amorphization process. The obtained results suggest that electrochemically formed amorphous Li$_2$MnSiO$_4$ has much higher electrical conductivity and Li$^+$ ions diffusibility than as-obtained in sol−gel process crystalline one.

© 2013 Elsevier B.V. All rights reserved.

1. Introduction

The family of dilithiumorthosilicates − Li$_2$MSiO$_4$ (M = Fe, Mn, Co) − has been recently studied as potential polyanionic cathode materials for new generation safe Li-ion batteries [1–23]. Two lithium ions per formula unit, which can be reversibly de-inserted, result in theoretical capacities up to 333 mAh g^{-1} [1,2]. Due to a presence of strong covalent Si−O bonds, lithium silicates exhibit high thermal and chemical stability. Furthermore, Li$_2$MSiO$_4$ materials are nontoxic and environmentally friendly. These exceptional properties combined with low production costs, could potentially allow to use lithium silicates in large scale applications (e.g., electric and/or hybrid vehicles batteries, smart grids). Unfortunately, like all of the polyanionic cathode materials, lithium silicates are electric insulators showing electrical conductivity at room temperature within the range of 10^{-12}–10^{-15} S cm^{-1} [4]. However, conductivity

of such materials can be improved, for example, by coating with conductive layers and/or grain downsizing [1,4,24−26]. As achieved in systems based on LiFePO$_4$, grain size decrease can provide shorter diffusion paths for Li$^+$ ions and, as a result, improve the material performance [27,28]. The goal of this research was to investigate electrochemical properties of C/Li$_2$MnSiO$_4$ in relation to changes in the long range ordering of the crystalline structure in the material.

2. Experimental

Li$_2$MnSiO$_4$ was synthesized using sol−gel Pechini type reaction [16–19]. Starting reactants were: LiCH$_3$COO·2H$_2$O (Aldrich), Mn(CH$_3$COO)$_2$·4H$_2$O (Aldrich), tetraethoxysilane (Aldrich), ethylene glycol (POCh), citric acid (POCh) and ethanol (POCh). The reactants were mixed in a following molar ratio 1:1:18:6:4:16 − Mn:Si:C$_2$H$_6$O$_2$:C$_6$H$_8$O$_7$:C$_2$H$_5$OH:H$_2$O. Lithium acetate was used in 20% weight excess. All the reactants were dissolved in a distilled water. The dissolution was performed in a glass reactor at 60 °C and under an inert atmosphere (Ar). After a

* Corresponding author. Tel.: +48 126632280; fax: +48 126340515.
E-mail address: molendam@chemia.uj.edu.pl (M. Molenda).

complete dissolution of the reactants, 0.1 ml of concentrated solution of HCl was added to initiate a reaction, then, the reactants were left for 24 h. The mixture was subsequently aged for 7 days at 60 °C. Obtained xerogel has been calcined in a tube furnace under a constant flow of argon at 600 °C for 12 h. To remove residues of carbonized organic matrix, obtained material has been heat treated at 400 °C for 4 h under an air flow. To prepare C/Li_2MnSiO_4 composite, Li_2MnSiO_4 was coated with carbon using poly-N-vinylformamide (PNVF) and 5–10 wt% pyromellitic acid (PMA) as a carbon polymer precursor [24,25,29]. Li_2MnSiO_4 grains were suspended in water polymer solution (8–15 wt%) and impregnated with carbon precursor. Finally, the samples have been dried up in an air drier at 90 °C for 24 h and pyrolyzed at 600 °C for 6 h under constant argon flow.

A carbon content in the C/Li_2MnSiO_4 composite was determined using temperature programmed oxidation (TPO) carried out in a Mettler-Toledo 851^e thermo-analyzer. Structural properties of the material were investigated using a BRUKER D2 PHASER X-ray powder diffractometer with a Cu lamp ($K\alpha_1$ radiation = 0.154060 nm). A morphology of the composite was observed using a transmission electron microscope (TEM, TECNAI G2 F20 200 kV). Electrochemical cells were prepared using a CR 2032 coin cell assembly in which the cathode material was placed on an aluminum current collector without using any binder. A metallic lithium foil was used as an anode. As a separating material, a combination of a microporous PP/PE/PP (Celgard 2325) and a porous glass microfiber filters (Whatman GF/F) was used. A 1 M solution of a $LiPF_6$ in an ethylene carbonate (EC)/dimethyl carbonate (DMC) (1:1) was used as an electrolyte. The galvanostatic cycling studies were carried out on an ATLAS 0961 MBI multichannel testing system, in a range of 1.5–4.8 V, at 0.02 and 0.06C rate, at room temperature (RT). Cyclic voltammetry (CV), as well as potentiostatic electrochemical impedance spectroscopy (EIS), were performed on a potentiostat/galvanostat AUTOLAB PGSTAT302N/FRA2. The CV scans were carried out at 1 and 0.1 mV s^{-1} scan rates in a range of 1.5–4.8 V, starting from an open circuit potential (OCP). The EIS measurements were conducted with 5 mV amplitude of an alternative current signal over the frequency range between 100 kHz and 10 mHz. The impedance was measured at different states of charge (SOC) of a cell. The cell was galvanostatically charged/discharged at 0.02C rate at RT.
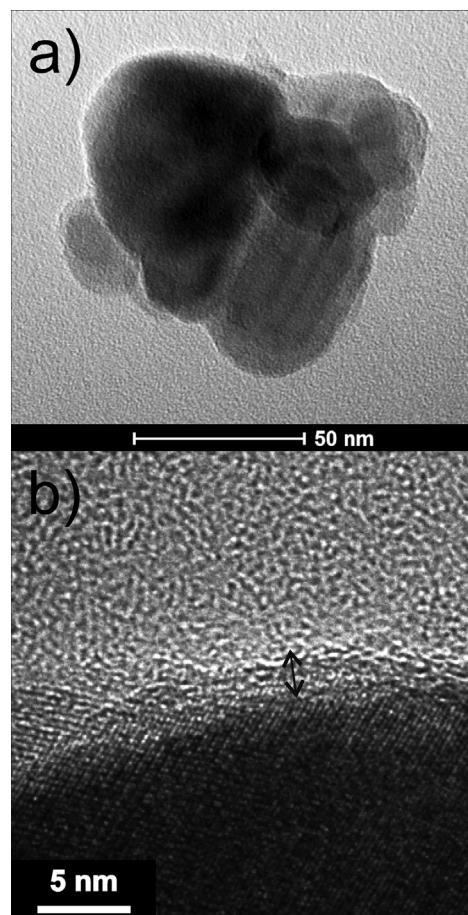

Fig. 2. Transmission electron microscope micrographs of C/Li_2MnSiO_4: a) bright field image of composite grains, b) high resolution micrograph with marked (black arrow) carbon coating covering active material.

3. Results and discussion

The carbon loading in the C/Li_2MnSiO_4 composite was calculated basing on the TPO measurements and it was estimated at
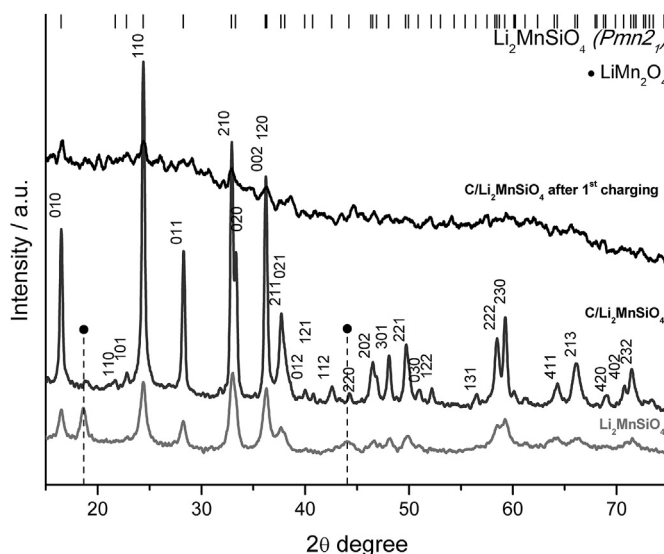

Fig. 1. X-ray diffraction patterns of Li_2MnSiO_4 obtained in sol–gel synthesis, carbon coated C/Li_2MnSiO_4 and ex-situ XRD patterns of C/Li_2MnSiO_4 composite after initial charging. Position of all $Pmn2_1$ Li_2MnSiO_4 lines are marked in the top of the figure.

17 wt%. XRD patterns of the Li_2MnSiO_4, the carbon coated material (C/Li_2MnSiO_4) and the C/Li_2MnSiO_4 after the initial charging are presented in a Fig. 1. The as-synthesized material consists of a $LiMn_2O_4$ impurities (19 and 44° 2θ diffraction lines) formed on the surface during the heat treatment in the air atmosphere. The carbon coating process causes a recombination of the Li_2MnSiO_4 phase. After coating, the Li_2MnSiO_4 ($Pmn2_1$) is a main phase in the C/Li_2MnSiO_4 material — all of the diffraction lines correspond to the Li_2MnSiO_4 phase, except for a very low intensity line around 19° 2θ. The obtained composite material is well-crystallized — its diffraction lines are sharp and intense. Average crystallite size, calculated from diffraction line broadening using Scherrer equation, is 25 nm. The XRD pattern of the C/Li_2MnSiO_4 after first charging still consist of some diffraction lines which can be associated with Li_2MnSiO_4 phase ((010), (011), (210), (002) reflections) but it is clear that the material structure has changed — long range order was destroyed. One may conclude that after first charging, the material undergoes amorphization, what is consistent with other reports concerning the electrochemical studies of the Li_2MnSiO_4 [2,14,19,30].

TEM micrographs (Fig. 2) show the morphology of the C/Li_2MnSiO_4 composite. Bright field micrograph (Fig. 2a) shows a group of crystallites of the Li_2MnSiO_4 coated with conductive carbon layer. The carbon coatings adhere well to the surface of the
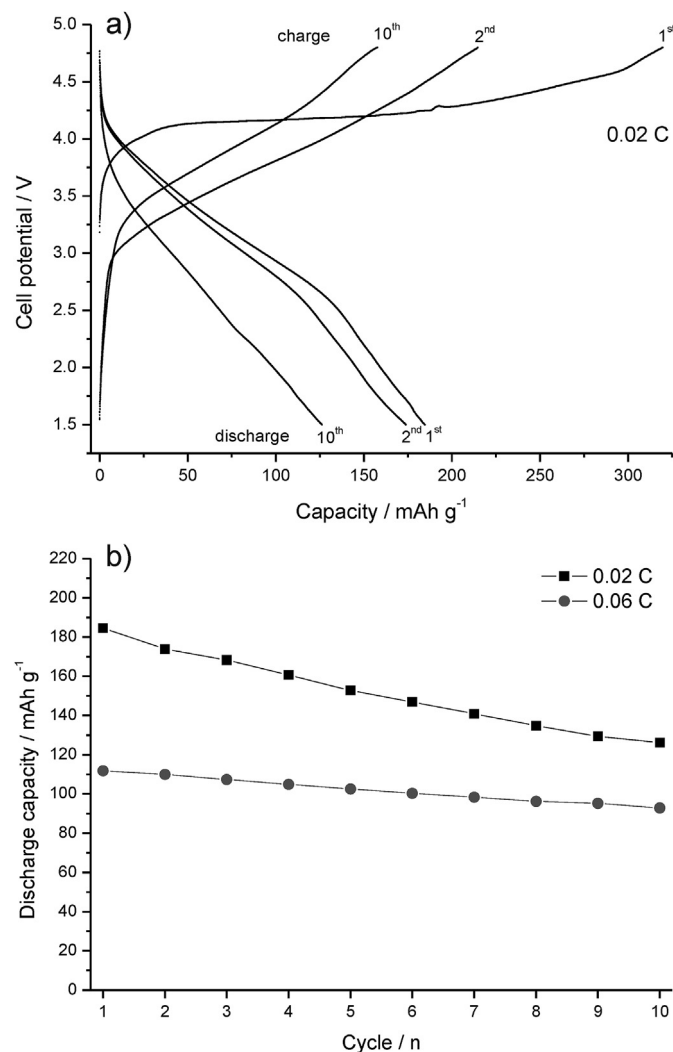

Fig. 4. Nyquist plot of electrochemical impedance spectroscopy (potentiostatic mode) for $Li/Li^+/(C/Li_2MnSiO_4)$ cell at different SOC.
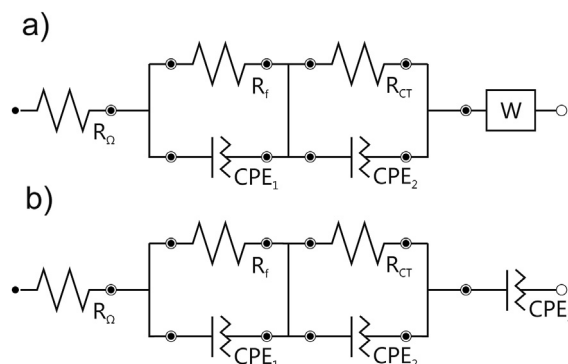
Fig. 5. Proposed equivalent circuits for EIS data fitting: a) before charging (3.1 V), b) after initial cycling (charged sample 4.8 V and discharged sample 1.5 V).

silicate grain, what can be observed in a high resolution micrograph (HREM — Fig. 2b). Due to the fact that the powder particles are placed on a carbon supporting film during TEM investigation, there is only a slight difference in contrast between the carbon layer deposited on the material (marked with an arrow) and a background (carbon support) of the micrograph. The carbon coating is about 4—5 nm thick and uniformly covers the active material grain. The TEM analysis allowed to observe that the obtained Li_2MnSiO_4 has a grain size in the range of 25—50 nm what corresponds well to crystallite size calculated from XRD measurement, suggesting only slight crystallites agglomeration.

Electrochemical performance of the C/Li_2MnSiO_4 composite during galvanostatic charge/discharge tests is presented in Fig. 3. Fig. 3a shows charge and discharge curves characteristic for a dilithium manganese orthosilicate. The first charging curve has a different shape from the following ones, which is related to the structural changes in the material. The initial charging process

Fig. 3. Galvanostatic cycling studies of $Li/Li^+/(C/Li_2MnSiO_4)$ cells: a) voltage profiles for sample cycled at 0.02C rate, b) discharge capacity of samples cycled at 0.02 and 0.06C rate.
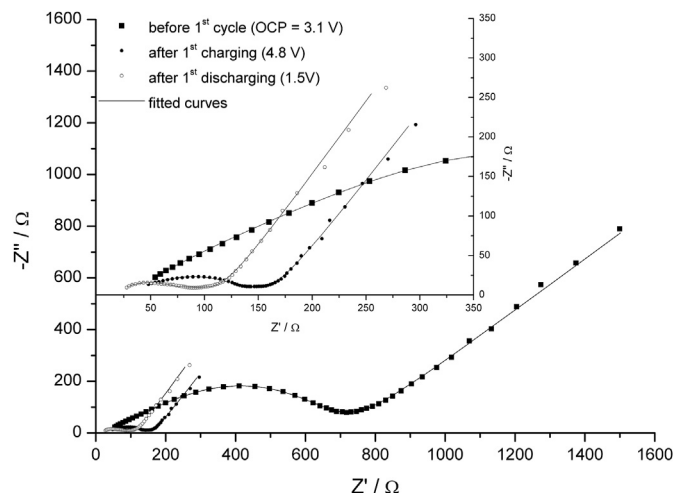
Table 1
Parameters of impedance measurements, calculated values of elements in proposed equivalent circuits and diffusion coefficient of lithium ion.

$Li/Li^+/(C/Li_2MnSiO_4)$	Potential [V]	R_Ω [Ω]	R_f [Ω]	R_{CT} [Ω]	D_{Li^+} [cm^2 s^{-1}]
Before charging	3.1	25.7	211	497	$3.4 \cdot 10^{-18}$
Charged	4.8	7.74	49.5	133	$3.5 \cdot 10^{-15}$
Discharged	1.5	15.5	40.2	68.5	$1.1 \cdot 10^{-16}$
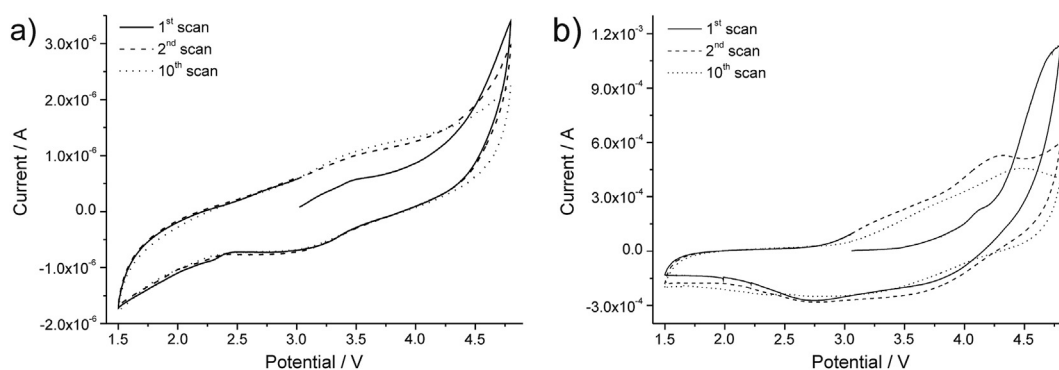
Fig. 6. First, second and tenth scans of cyclic voltammetry of Li/Li$^+$/(C/Li$_2$MnSiO$_4$) cell measured at: a) 1 mV s^{-1} and b) 0.1 mV s^{-1} scan rate.

consumes a charge nearly equal to the theoretical capacity of the active material ($\sim$330 mAh g^{-1}), however, a part of this charge is being consumed in a solid electrolyte interface (SEI) formation process. The first discharge capacity (185 mAh g^{-1}) corresponds to a reversible insertion of more than one lithium-ion per formula unit (1.11 mole Li$^+$). While next cycles cause discharge capacity fading, down to about 130 mAh g^{-1} (70% of initial discharge capacity) after 10th cycle (0.02C rate). The capacity of the material cycled at a slightly higher C rate (0.06) is characterized by a 17% drop of initial discharge capacity (112 mAh g^{-1}) after 10 cycles, and equals 93 mAh g^{-1}. It's worth to notice that smaller capacity fading was observed for higher working currents, what may suggest that a stable reversible capacity is obtained in case of an amorphous – glass-like Li$_2$MnSiO$_4$.

To understand the observed changes in the material which occur during the initial charging, EIS measurements were conducted at different SOCs: before first charging (at open circuit potential OCP = 3.1 V), after first charging (at 4.8 V) and after first discharging (at 1.5 V). Fig. 4 shows a Nyquist plot of a Li/Li$^+$/(C/Li$_2$MnSiO$_4$) cell with curves fitted basing on a Boukamp model using Nova 1.8 AUTOLAB software. The fitting was performed for equivalent circuits presented in Fig. 5. Calculated values of each resistor are collected in Table 1. The electrical resistance in the cell drastically decreases after the initial charging. This effect may be connected with the morphological changes in both the active material and the coating layers. A shift of the plots in the Z′ (real) axis (high frequency region) is associated with the resistance of electrical contacts in the cell, electrolyte and separators and it is represented as an R_Ω in the equivalent circuits. First semicircle (high frequency region) corresponds to a lithium ion diffusion (R_f) through conductive carbon layer (in the cell before cycling) and the carbon coating with formed SEI (plots after charging and discharging). A decrease of R_f after charging can be explained by a carbon layer modification causing formation of lithium easy diffusion paths through the carbon coating. Subsequent discharging process does not affect the resistance of the coating layers what confirms stability of the carbon coating. Second semicircle (medium frequency region) describes resistance of the charge transfer (R_{CT}). The values of R_{CT} suggest that the amorphous material reveals higher electrical conductivity than the crystalline Li$_2$MnSiO$_4$. Furthermore, a continuous decrease of the R_{CT} value after discharging indicates that the amorphization process is not completed during the initial charging. Tail lines present at a low frequency are connected with a Li$^+$ migration in the active material. The tail line in the EIS spectrum of the cell before charging has a slope around 45° to the real axis and is represented by a Warburg element (constant phase element – CPE with constant phase of 45°) in the equivalent circuit. For measurements performed after charging/discharging CPE with different than 45° phase is more suitable to

describe the Li-ion diffusion in the material, therefore the Warburg element (W) was replaced with a CPE$_3$ (constant phase ca. 62°) in the circuit 6b. In Table 1 diffusion coefficient of lithium calculated from impedance data using Warburg factor [31] is presented. Similarly to changes of R_{CT} values during the amorphization of material a significant increase of diffusion coefficient of lithium ion is observed, from 3.4·10^{-18} to 1.1·10^{-16} cm^2 s^{-1} after first charge/discharge cycle. The observed diffusion coefficient of lithium ion after first charging was higher and equal to 3.5·10^{-15} cm^2 s^{-1}.

A cyclic voltammetry was carried out in the range of 1.5–4.8 V at 1 mV s^{-1} scan rate (Fig. 6a) and 0.1 mV s^{-1} (Fig. 6b) starting from OCP = 3 V. Fig. 6 presents first, second and tenth CV scan obtained at two different scan rates. Due to diffusion limitations in the active material, voltammogram obtained with higher scan rate (Fig. 6a) has no obvious oxidation peak. Redox reactions on these CV curves are represented by shoulder shape region at around 4 V [32]. Slowing down the scan rate to 0.1 mV s^{-1} allows to observe week but clearly visible oxidation peaks (Fig. 6b). Position of oxidation peak at about 4.2 V corresponds well with voltage plateau measured during galvanostatic studies. It can be seen that after the initial charging currents transferred throughout the material (3–4.2 V region) are twice as high as in the case of the first scan. In both cases (fast and low CV scan rate) material amorphization during lithium deintercalation resulted in enhancement of redox peaks suggesting improvement of Li$^+$ ions diffusibility. These results are consistent with the EIS measurements which showed an increase in conductivity and diffusion coefficient of lithium ion in the material.

4. Conclusions

The nanosized Li$_2$MnSiO$_4$ was successfully produced in the sol–gel Pechini's synthesis. The carbon coatings formed using polymer precursors revealed high stability and provided good electrical properties of the C/Li$_2$MnSiO$_4$ composite. The ex-situ XRD measurements performed after first charging confirmed amorphization of the active material during the electrochemical cycling. The EIS and CV studies showed that the electrical conductivity and diffusion coefficient of lithium ion of the amorphous active material is significantly higher than that of the starting one. It seems that within the whole working range of potential (1.5–4.8 V) it is possible to de-insert reversibly only one lithium-ion per formula unit what is followed by destruction of long range ordering in the material. Amorphization rate can be accelerated by higher working currents conditions. The material reveals a high reversible capacity (185 mAh g^{-1} in the first discharge at 0.02C rate – 1.11 mole Li$^+$) slightly exceeding the theoretical capacity of the material for one electron process.

Acknowledgments

References

[1] M.E. Arroyo-de Dompablo, M. Armand, J.M. Tarascon, U. Amator, Electrochem. Commun. 8 (2006) 1292—1298.
[2] Z.L. Gong, Y.X. Li, Y. Yang, J. Power Sources 174 (2007) 524—527.
[3] A. Nyten, A. Abouimrane, M. Armand, T. Gustafsson, J.O. Thomas, Electrochem. Commun. 7 (2005) 156—160.
[4] A. Kokalj, R. Dominko, G. Mali, A. Meden, M. Gaberscek, J. Jamnik, Chem. Mater. 19 (2007) 3633—3640.
[5] C. Sirisopanaporn, A. Boulineau, D. Hanzel, R. Dominko, B. Budic, A.R. Armstrong, P.G. Bruce, C. Masquelier, Inorg. Chem. 49 (2010) 7446—7451.
[6] A. Boulineau, C. Sirisopanaporn, R. Dominko, A.R. Armstrong, P.G. Bruce, C. Masquelier, Dalton Trans. 39 (2010) 6310—6316.
[7] C. Sirisopanaporn, C. Masquelier, P.G. Bruce, A.R. Armstrong, R. Dominko, J. Am. Chem. Soc. 133 (2011) 1263—1265.
[8] G. Mali, M. Rangusa, C. Sirisopanaporn, R. Dominko, Solid State Nucl. Magn. Reson. 42 (2012) 33—41.
[9] W. Liu, Y. Xu, R. Yang, J. Alloy Compd. 480 (2009) L1—L4.
[10] N. Kuganathan, M.S. Islam, Chem. Mater. 21 (2009) 5196—5202.
[11] K. Karthikeyan, V. Aravindan, S.B. Lee, I.C. Jang, H.H. Lim, G.J. Park, M. Yoshio, Y.S. Lee, J. Power Sources 195 (2010) 3761—3764.
[12] R.J. Gummow, N. Sharma, V.K. Peterson, Y. He, J. Solid State Chem. 188 (2012) 32—37.
[13] R.J. Gummow, N. Sharma, V.K. Peterson, Y. He, J. Power Sources 197 (2012) 231—237.
[14] R. Dominko, M. Bele, A. Kokalj, M. Gaberscek, J. Jamnik, J. Power Sources 174 (2007) 457—461.
[15] R. Dominko, M. Bele, M. Gaberscek, A. Meden, M. Remskar, J. Jamnik, Electrochem. Commun. 8 (2006) 217—222.
[16] Y.X. Li, Z.L. Gong, Y. Yang, J. Power Sources 174 (2007) 528—532.
[17] I. Belharouak, A. Abouimrane, K. Amine, J. Phys. Chem. C 113 (2009) 20733—20737.
[18] M. Molenda, M. Swietoslawski, A. Rafalska-Lasocha, R. Dziembaj, Funct. Mater. Lett. 4 (2011) 135—138.
[19] V. Aravindan, S. Ravi, W.S. Kim, S.Y. Lee, Y.S. Lee, J. Colloid Interf. Sci. 355 (2011) 472—477.
[20] M. Swietoslawski, M. Molenda, M. Zaitz, R. Dziembaj, ECS Trans. 41 (2012) 129—137.
[21] V. Aravindan, K. Karthikeyan, K.S. Kang, W.S. Yoon, W.S. Kim, Y.S. Lee, J. Mater. Chem. 21 (2011) 2470—2475.
[22] S. Zhang, Y. Li, G. Xu, S. Li, Y. Lu, O. Toprakci, X. Zhang, J. Power Sources 213 (2012) 10—15.
[23] R. Dominko, I. Arcon, A. Kodre, D. Hanzel, M. Gaberscek, J. Power Sources 189 (2009) 51—58.
[24] M. Molenda, R. Dziembaj, M. Drozdek, E. Podstawka, L.M. Proniewicz, Solid State Ionics 179 (2008) 197—201.
[25] M. Molenda, R. Dziembaj, E. Podstawka, L.M. Proniewicz, Z. Piwowarska, J. Power Sources 174 (2007) 613—618.
[26] J. Moskon, R. Dominko, R. Cerc-Korosec, M. Gaberscek, J. Jamnik, J. Power Sources 174 (2007) 683—688.
[27] M. Gaberscek, R. Dominko, J. Jamnik, Electrochem. Commun. 9 (2007) 2778—2783.
[28] Jin-Ming Chen, Chia-Haw Hsu, Yu-Run Lin, Mei-Hui Hsiao, Ting-Kuo Fey George, J. Power Sources 184 (2008) 498—502.
[29] M. Molenda, R. Dziembaj, A. Kochanowski, E. Bortel, M. Drozdek, Z. Piwowarska, Process for the Preparation of Conductive Carbon Layers on Powdered Supports, Int. Patent Appl. No. WO 2010/021557, US Patent Application 20110151112.
[30] M.E. Arroyo-de Dompablo, R. Dominko, J.M. Gallardo-Amores, L. Dupont, G. Mali, H. Ehrenberg, J. Jamnik, E. Moraacute;n, Chem. Mater. 20 (2008) 5574—5874.
[31] X.Y. Wang, H. Hao, J.L. Liu, T. Huang, A. Yu, Electrochim. Acta 56 (2011) 4065—4069.
[32] I. Streeter, R.G. Compton, J. Phys. Chem. C 111 (2007) 18049—18054.